

Comprehensive Evaluation of Cryopreserved Bone-Derived Osteoblasts for the Repair of Segmental Mandibular Defects in Canines

Shaoyi Wang, DDS, PhD;* Jun Zhao, DDS, PhD;† Wenjie Zhang, PhD;‡ Dongxia Ye, DDS, PhD;§ Xiaochen Zhang, PhD;* Duohong Zou, DDS, PhD;* Xiuli Zhang, PhD;§ Xiaojuan Sun, DDS, PhD;¶ Shuyang Sun, DDS, PhD;* Weijie Zhang, MS;* Chi Yang, DDS, MD;* Xinquan Jiang, DDS, MD, PhD;** Zhiyuan Zhang, DDS, MD*

ABSTRACT

Background: The repair of segmental mandibular defects remains challenging in the clinic. Previous studies have shown that cryopreserved bone-derived osteoblasts (CBOs) have good proliferation and osteogenicity. However, whether these cells can be used in the repair of segmental mandibular defects is largely unknown.

Purpose: In this study, we applied CBOs combined with beta-tricalcium phosphate (β -TCP) to repair a segmental mandibular defect in canines and thus established the feasibility of using this type of tissue-bank cell for the repair of large bone defects in the future.

Material and Methods: Sixteen segmental mandibular defects in 16 animals were made on the right side. Sequential radiographs, computer tomography, polychrome fluorescent labeling, immunohistochemical staining, and histological analysis were used to evaluate the effects of tissue-engineered bone for segmental mandibular defects.

Results: Our results demonstrated that CBOs combined with β -TCP promoted bone mineralization and deposition at the early stage, and bony union was achieved in the CBO and fresh bone-derived osteoblast (FBO) groups. However, nonunion and minimal callus were present in the β -TCP group. Furthermore, there was a large amount of newly formed bone in the CBO and FBO groups and in the autogenous bone group. Additionally, osteocalcin immunohistochemistry showed intensive osteocalcin immunoreactivity in the bone matrix of the CBO and FBO groups.

Conclusions: These data indicate that CBOs implanted in a scaffold can promote new bone formation, and this tissue-engineered bone can repair critically sized segmental mandibular defects in canines. The use of CBOs combined with β -TCP may be an effective approach for the reconstruction of segmental mandibular defects in the clinic.

KEY WORDS: bone regeneration, cryopreserved bone-derived osteoblasts, segmental mandibular defect, tissue banking

*Department of Oral and Maxillofacial Surgery, Ninth People's Hospital, Shanghai Jiao Tong University School of Medicine, Shanghai Key Laboratory of Stomatology, Shanghai, China; †Department of Orthodontics, Ninth People's Hospital, Shanghai Jiao Tong University School of Medicine, Shanghai Key Laboratory of Stomatology, Shanghai, China; ‡Department of Prosthodontics, Ninth People's Hospital, Shanghai Jiao Tong University School of Medicine, Shanghai Key Laboratory of Stomatology, Shanghai, China; §Shanghai Research Institute of Stomatology, Ninth People's Hospital, Shanghai Jiao Tong University School of Medicine, Shanghai Key Laboratory of Stomatology, Shanghai, China; ¶Department of Oral and Maxillofacial Surgery, Affiliated Hospital of Ningxia Medical University, Ningxia, China; **Oral Bioengineering Lab/Regenerative Medicine Lab, Department of Prosthodontics, Shanghai Research Institute of Stomatology, Ninth People's Hospital, Shanghai Jiao Tong University School of Medicine, Shanghai Key Laboratory of Stomatology, Shanghai, China

INTRODUCTION

The repair of segmental mandibular defects is often required in patients because of tumor resection, trauma, infection, or congenital malformation. Autogenous bone grafts have osteogenic, osteoconductive, and osteoinductive properties, and they are thus considered to be the "gold standard" grafting material for the reconstruction of minor and major bony defects.^{1,2} The disadvantages of this approach include prolonged

Reprint requests: Dr. Zhiyuan Zhang, No: 639, Zhi-zao-ju road, 200011, Shanghai, China; e-mail: zhzy@omschina.org.cn

© 2013 Wiley Periodicals, Inc.

DOI 10.1111/cid.12164

operation time, limited autograft quantity, and donor site morbidity.³ One possibility for addressing these disadvantages is to generate bioartificial bone tissues through tissue engineering.^{4,5} Among seeded cells, artificially created materials, and physiologically active substances in tissue engineering, seeded cells have become an integral part of this strategy.^{6,7}

In the past decades, researchers have explored a variety of cells, including bone marrow mesenchymal stem cells, adipose-derived stem cells, and muscle-derived stem cells, for tissue regeneration in animal and clinical studies.^{8–12} Although the characteristics of fresh tissue-derived cells have been studied in detail, frozen bone-derived cells are still poorly understood.^{13,14} The viability of osteoblasts in bone tissue was reported to be maintained by slow cooling with a cryoprotectant and rapid thawing.^{15,16} Therefore, the transplantation of cryopreserved bone-derived osteoblasts (CBOs) may hold promise for eventual application in bone regeneration.

In previous studies, we isolated living CBOs from banked tissue and demonstrated that CBOs could be acquired easily, with a good proliferative activity and an osteogenic phenotype. Our group has shown that CBOs could be used as a new cell source for tissue engineering and regenerative medicine because they meet generally accepted standards as seeded cells.¹⁷ However, whether these cells can be applied in the reconstruction of segmental mandibular defects in a large animal model is still largely unknown.

Beta-tricalcium phosphate (β -TCP) is a synthetic and biodegradable ceramic material with good biocompatibility and osteoconductivity that has been commonly used in various applications in oral and maxillofacial surgery, such as alveolar ridge augmentation, sinus floor augmentation, and benign bone tumor filling.^{18–20} In this study, we designed a protocol to apply CBOs combined with β -TCP to repair segmental mandibular defects in a canine model. We monitored the bone mineralization and deposition of the CBOs in large-volume bone regeneration and thus established the feasibility of using this type of tissue-bank cell for clinical applications in the future.

MATERIALS AND METHODS

Ethics Statement

The Ethics Committee for Animal Research at the Ninth People's Hospital affiliated with Shanghai Jiao

Tong University approved all the experimental protocols involving the use of dogs.

Animals

In this study, 16 male beagle dogs in a healthy condition, aged 12 to 18 months old with an average weight of 12.5 kg, were obtained from the Laboratory Animal Center of Shanghai Jiao Tong University.

Cryopreservation and Cell Culture

Bone fragments were acquired, processed, and stored as described previously.¹⁷ Briefly, bone fragments (diameter 1–1.5 mm) were acquired from the mandible in adult beagle dogs and transferred into 1.5 mL cryotubes containing cryoprotectant, which were first stored in a refrigerator at -80°C for 30 minutes. Then the tubes were placed in storage at -196°C in liquid nitrogen. The frozen bone chips were thawed and incubated with standard Dulbecco's modified Eagle's medium containing 10% (v/v) fetal bovine serum (Hyclone, Logan, UT, USA) after a prescribed 3 months of cryopreservation. The cell culture method was performed in accordance with a previous report.¹⁷ The medium was replaced every 3 to 4 days until cell density reached 70% to 80% confluence. After the first passage, the following three supplements were added: 100 nM dexamethasone, 0.05 mM ascorbic acid 2-phosphate, and 10 mM beta-glycerophosphate. The cells were then incubated continuously at 37°C in a humidified atmosphere of 95% air and 5% CO_2 . Cells at passages 2 to 3 were used for the experiments that follow. Each experiment was repeated four times. The study protocol is shown in Figure 1. Cell proliferation was assessed by flow cytometric analysis using propidium iodide according to the manufacturer's instructions on a FACSCalibur device (Becton, Dickinson and Co., Franklin Lakes, NJ, USA).

Alkaline Phosphatase and Alizarin Red S Calcium Nodule Staining

To evaluate the level of mineralization, alkaline phosphatase activity and alizarin red S calcium nodule staining were evaluated according to previous reports.^{21–23} The alkaline phosphatase activity of the CBOs was evaluated after they were cultured for 14 days. The cells were fixed for 10 minutes at 4°C and incubated with a mixture of naphthol AS-MX phosphate and fast blue BB salt (alkaline phosphatase kit, Hongqiao, Shanghai, China). Areas stained purple were designated as positive.

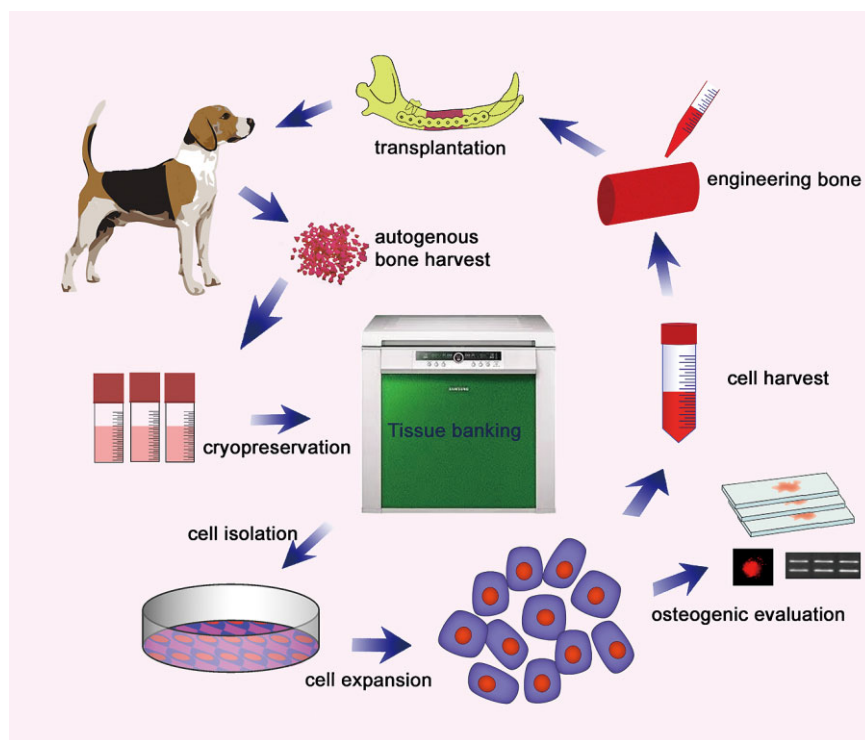


Figure 1 Schematic diagram showing the application of cryopreserved bone-derived osteoblasts (CBOs) for bone regeneration, which included bone harvest, cryopreservation of dog bone fragments, CBO isolation and expansion, and osteogenic evaluation in vitro and in vivo.

Calcium nodules were stained by culturing the cells with 10 mg/L alizarin red S (Sigma Aldrich, St. Louis, MO, USA) for 5 to 7 days before observation under a fluorescence microscope (Leica DM1RB, Leica Microsystems, Wetzlar, Germany).

Reverse Transcription-Polymerase Chain Reaction

Based on a previous report, the transcription of osteogenic genes, including collagen I (Col I), osteocalcin (OCN), osteopontin (OPN), and bone sialoprotein (BSP), was detected by reverse transcription-polymerase chain reaction (RT-PCR).²⁴ Highly purified gene-specific primers for Col I, OCN, OPN, BSP, and a calibrator reference gene (beta-actin) were synthesized commercially (Shengong Co. Ltd., Shanghai, China), and the specific primers were as follows: beta-actin, sense 5'-CCTGTGGCATCCACGAAACT-3' and antisense 5'-GAAGCATTTGCGGTGGACGA-3' (product size 307 bp); Col I, sense 5'-CCAAGAAGAAGACATCCCACC-3' and antisense 5'-CAGATCACGTCATCGACAA-3' (product size 135 bp); OCN, sense 5'-TCACAGACCCAGACAGAACCG-3' and antisense 5'-AGCCCAGAGTCCAGGTAGCG-3' (product size

207 bp); OPN, sense 5'-CACTGACATTCCAGCAAC-3' and antisense 5'-ATCTTCCATACTCGCACT-3' (product size 190 bp); BSP, sense 5'-TGGCTCTAAGACAACACTC-3' and antisense 5'-TGTGCCCTTTATAGTAGCT-3' (product size 245 bp).

Immunohistochemical Staining for Osteocalcin and Osteopontin

Immunohistochemical staining was used to determine the protein expression of OCN and OPN in CBOs and fresh bone-derived osteoblasts (FBOs). As previously reported,¹⁷ the cells were seeded and grown on cover glass for 4 days and then incubated with mixed primary antibodies (mouse polyclonal antibodies against OCN or rabbit polyclonal antibodies against OPN; Abcam, Cambridge, UK) at a dilution of 1:100. Then, green fluorescent-labeled goat anti-mouse and red fluorescent-labeled goat anti-rabbit secondary antibodies (Invitrogen, CA, USA) were applied. The slides were observed using a confocal laser scanning microscope, and three-dimensional structures were reconstructed from a series of fluorescent images after the nuclei were stained with Hoechst 33342.

Preparation of CBOs/ β -TCP Constructs

β -TCP scaffolds (Shanghai Bio-Lu Biomaterials Co. Ltd., Shanghai, China) were molded into cuboids (30 mm \times 7 mm \times 10 mm) and sterilized with epoxy ethane before use. For cell seeding, the CBOs were detached from the culture dishes, centrifuged to remove the supernatant, and then resuspended in culture medium without serum at a density of 2×10^7 cells/mL. Cells in suspension were slowly added to β -TCP cuboids until reaching saturation (0.6 mL of cell suspension). After incubation for an additional 4 hours, the CBO/ β -TCP constructs were implanted in vivo.

Surgical Procedure

Animals were anesthetized through an intramuscular injection of ketamine (10 mg/kg) and xylazine (4 mg/kg), and the bilateral maxillary and mandibular premolar and molar teeth as well as the mandibular canine were extracted 4 months before the transplantation surgeries. Sixteen segmental mandibular defects in 16 animals were made on the right side and randomly repaired according to the following four groups: Group A (CBOs/ β -TCP, $n = 4$), Group B (FBOs/ β -TCP, $n = 4$), Group C (resected autogenous mandibular segments, $n = 4$), and Group D (β -TCP alone, $n = 4$). In Groups A and B, the CBOs and FBOs were acquired from cryopreserved/fresh autogenous bone.

Under general anesthesia, the inferior mandibular border was exposed through a submandibular skin incision. The mandibular periosteum was carefully dissected and removed. After adjustment of the titanium plate and titanium mesh, a segmental mandibular defect with a length of 30 mm was made at the midportion of the mandible. The neurovascular bundle was ligated. Then, the titanium plate and titanium mesh were secured in place with titanium screws. The bone defect was filled with CBOs/ β -TCP, FBOs/ β -TCP, resected autologous mandibular segments, or β -TCP alone. The incisions were closed with 3-0 silk suture. The titanium plates and titanium mesh were removed 11 months after the surgery. All animals were maintained on a soft diet during the study and sacrificed at 12 months after the surgery.

Sequential Fluorescent Labeling

Sequential fluorescent labeling permitted a more detailed analysis of sequential information regarding the accretion and direction of bone formation, as well as an assessment of the time course of new bone formation

and mineralization. At 2, 4, 7, and 11 months after the operation, the animals were intraperitoneally administered 25 mg/kg tetracycline hydrochloride (TE; Sigma), 30 mg/kg alizarin red S (AL), 20 mg/kg calcein (CA; Sigma), and 30 mg/kg calcein blue (CB; Tokyo Chemical Industry, Toyko, Japan), respectively.

Radiographic Observation

To evaluate scaffold degradation and new bone formation and mineralization at 1, 5, and 11 months post-operation, mandibular radiographs were obtained using a dental x-ray machine (Trophy, Marne La Vallee Cedex 2, France) from a distance of 7 cm (230 V, 8 mA) with an exposure time of 0.28 seconds. Maxillofacial CT images were also obtained by multislice spiral CT (GE Lightspeed Ultra 16, General Electric, Milwaukee, WI, USA) at 3 days before sacrifice.

Sample Preparation and Immunohistochemical Staining

The specimens were bisected in the mesiodistal direction, cut into buccal and lingual halves, and then fixed in 10% buffered formalin (pH 7.4). One half was decalcified, embedded in paraffin, sectioned at 4 μ m, and processed for immunohistochemical staining. The other half was embedded in polymethylmethacrylate and sectioned at 150 μ m using a microtome (Leica Biosystems, Nussloch, Germany); the sections were subsequently ground and polished to a final thickness of approximately 70 μ m. Fluorescent labeling was then observed using confocal scanning laser microscopy.

The expression of OCN in decalcified specimens was evaluated using immunohistochemistry. Briefly, the slides were deparaffinized through a series of xylene baths and rehydrated using graded concentrations of ethanol. Then, endogenous peroxidase was inactivated by treatment with 3% hydrogen peroxide for 10 minutes. To restore antigenicity, tissue sections were incubated with 0.1% trypsinase for 30 minutes at 37°C, followed by incubation with 1% (v/v) bovine serum albumin for 30 minutes at room temperature. The slides were then incubated with a mouse monoclonal antibody against OCN, followed by incubation with a goat anti-mouse secondary antibody for 30 minutes at room temperature. Staining was performed using diaminobenzidine substrate (Boster Co. Ltd., Wuhan, China). The sections were counterstained with

hematoxylin, dehydrated through a series of alcohols and xylene, and then mounted with mounting medium.

Histological Analysis

Bone mineralization and deposition at different time points could be detected through fluorescent labeling under a confocal laser scanning microscope. The excitation/emission wavelengths of each of the fluorescent molecules were as follows: 405/580 nm (TE, yellow), 488/517 nm (CA, green), 543/617 nm (AL, red), and 405/435 nm (CB, blue).²⁴ A three-dimensional fluorescent structure was reconstructed using a series of fluorescent images for TE, AL, CA, and CB, and the images for the four fluorescent labels were merged to reflect the mineralization of the regenerated bone. The images were evaluated separately for yellow (TE), red (AL), green (CA), and blue (CB).²⁵ The data obtained in the four-color fluorescent staining represented bone regeneration and mineralization at 2, 4, 7, and 11 months, respectively.

Finally, the sections were stained with Van Gieson's picrofuchsin for histologic observation. Measurement of the undecalcified specimens was performed using ImagePro Plus 6.0 (Media Cybernetics, Silver Spring, MD, USA). Three randomly selected sections from serial sections collected from each sample were analyzed. The proportion of newly formed bone within the segmental mandibular defect was calculated at low magnification ($\times 1.25$).

Statistical Analysis

Statistically significant differences ($p < .05$) among the groups were determined by ANOVA and Student-Newman-Keuls post hoc analysis or the Kruskal-Wallis nonparametric procedure followed by the Mann-Whitney *U* test for multiple comparisons based on the normal distribution and equal variance assumption tests. All statistical analyses were conducted using the SAS 6.12 statistical software package (SAS Institute, Cary, NC, USA). All data are presented as the mean \pm standard deviation.

RESULTS

Cell Culture

Approximately 5 to 9 days after the initial plating of the bone fragments, CBO outgrowth was observed, and the cells then proliferated quickly to reach confluence in another 4 to 5 days (Figure 2A). After subculture, the

cells showed a polygonal or a dendritic morphology and were used for further studies. Flow cytometry demonstrated that the percentage of cells existing in the G0/G1 phases and that existing in the S/G2/M phases were $83.85 \pm 5.34\%$ and $14.15 \pm 2.06\%$ ($n = 4$), respectively, which suggested that the CBOs maintained a viable state and proliferated well (Figure 2B).

Alkaline Phosphatase and Alizarin Red S Calcium Nodule Staining

After two weeks of culture in osteogenic medium, alkaline phosphatase expression of the CBOs was revealed by purple to dark red granules observed under light microscopy. Mineralized calcium nodules stained by alizarin red S were observed in the expanded cells, which showed red fluorescence under a fluorescence microscope (Figure 2C and D). These results suggested that the CBOs had good osteogenic potential after *in vitro* amplification.

Expression of Osteogenic Genes

RT-PCR demonstrated transcription of Col I, OCN, OPN, and BSP in the CBOs (Figure 2E). OCN and OPN protein expression was also confirmed by fluorescent immunohistochemistry in CBOs (Figure 2F) at levels comparable to those in FBOs (Figure 2G). All of the results above indicated that the CBOs maintained a definite osteoblastic phenotype after bone cryopreservation.

General Observations and Radiographic Analyses

All animals survived the surgical procedure with slight edema 4 to 6 days after the surgery and recovered rapidly from surgery with no indication of infection or other complications.

Using radiographs taken regularly, we monitored bone formation and remodeling at 1, 5, and 11 months post-operation. Though bone regeneration is hard to detect in radiographs because of the radiopacity of the scaffold and bone blocks and the scattering from the titanium mesh, it can still be used to preliminarily evaluate new bone formation. Representative radiographs of each group are shown in Figure 3 (arrows show the gaps between the graft and the original bone). At 1 month post-operation, the implants in Groups A, B, and D were radiopaque because of the presence of the β -TCP scaffold itself. There were gaps between the implants and host bones. At 5 months after surgery, in Groups A and

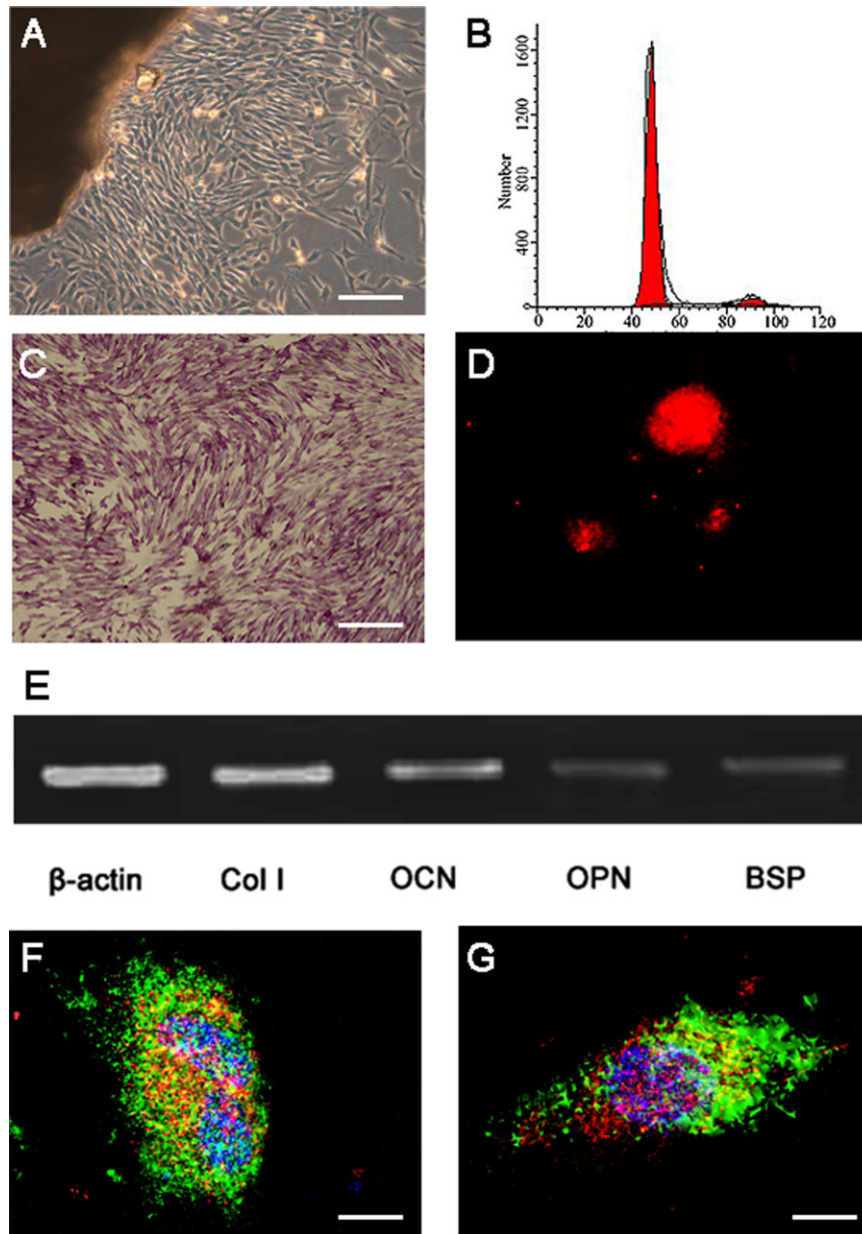


Figure 2 Cryopreserved bone-derived osteoblasts (CBOs) were cultured and displayed the typical dendritic, polygonal shape (A); scale bar = 40 μm . The cellular cycle demonstrated that the CBOs maintained a viable state and proliferated well (B). Alkaline phosphatase-positive staining, as shown by cells stained with purple to dark red granules (C); scale bar = 40 μm . Alizarin red S staining of mineralized calcium nodules was visible under a fluorescence microscope (D). Expression of osteogenic genes (collagen I [Col I], osteocalcin [OCN], osteopontin [OPN], and bone sialoprotein [BSP]) was observed in the CBOs (E). Three-dimensional reconstruction images of OCN (green) and OPN (red) fluorescence immunohistochemistry of CBOs (F) and fresh bone-derived osteoblasts (G); scale bar = 4 μm .

B, radiopacity was observed in the gaps, and the implants and host bones were integrally connected. The interfaces between the implants and host bones were difficult to distinguish. However, in Group D, which received β -TCP alone, the degradation was evident, based on the appearance of a radiotranslucent area around the implant, and the gap increased at this time point. At 11 months post-operation, the radiopacity of

the newly formed bone was highly increased, and bony union was achieved in Groups A and B. No difference was found between the CBO and FBO groups. In contrast, in Group D, the scaffold material had largely degraded, and bone nonunion was observed, with only minimal calluses detected.

In Group C, a radiolucent zone at the gap was still obvious at 1 month post-operation. At 5 months

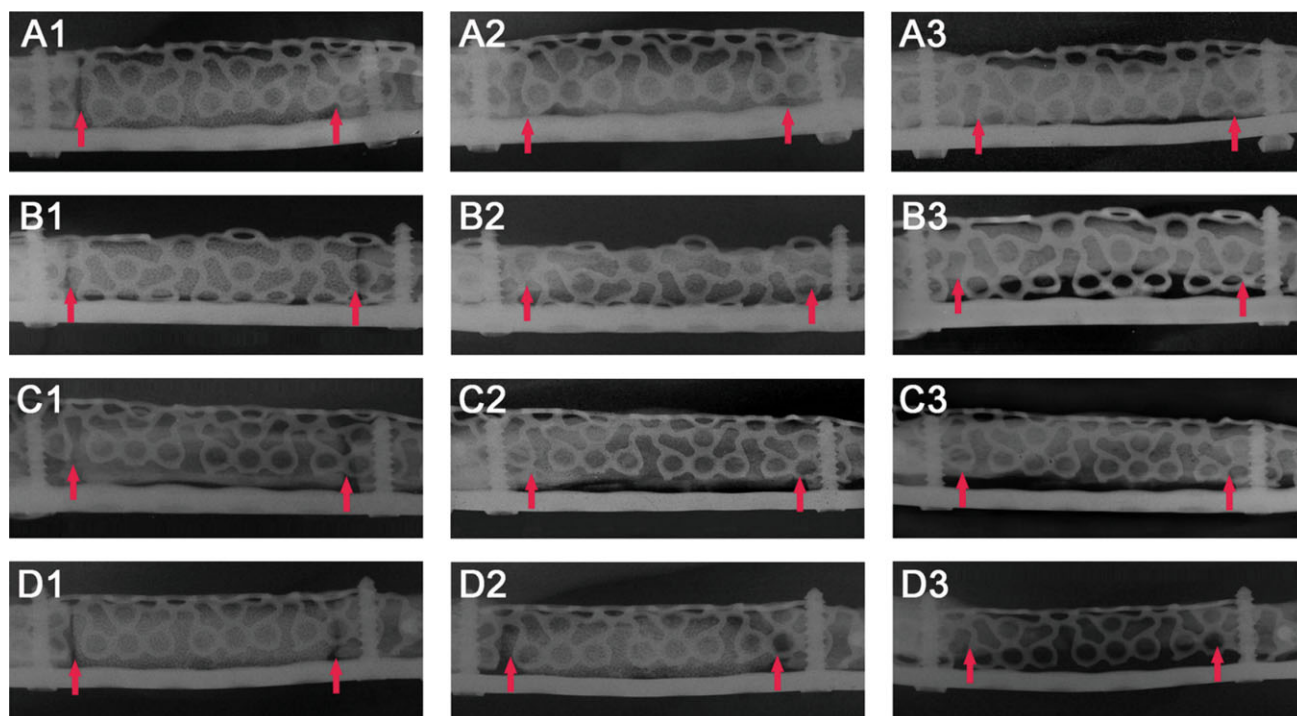


Figure 3 Radiographs of Groups A (A), B (B), C (C), and D (D) obtained at 1, 5, and 11 months post-operation. At 1 month post-operation, the implants in Groups A, B, C and D were radiopaque, and there were gaps between the implants and host bones (column 1). At 5 months after surgery in Groups A, B, and C, radiopacity was observed in the gaps, and the implants and host bones were integrally connected (A–C, column 2). In Group D, the degree of degradation was evident based on the appearance of a radiotranslucent area around the implant, and the gap increased at this time point (D2). At 11 months post-operation, bony union was achieved in Groups A, B, and C (A–C, column 3). In Group D, the beta-tricalcium phosphate was largely degraded, and bone nonunion with only a minimal callus was detected (D3). Arrows show the gaps between the graft and the original bone.

post-operation, the gap could no longer be easily discriminated on the radiographs because of new bone formation. At 11 months post-operation, the implant appeared smoother and more radiopaque, which indicates that new bone formation and remodeling was still occurring.

To determine the three-dimensional structure of the repaired mandibles, three-dimensional CT images from each group are presented in Figure 4. In Groups A, B, and C, bony union and complete continuity of the mandibular body were observed (Figure 4A–C). However, in the group that received β -TCP alone, the mandible presented a discontinuous appearance (Figure 4D).

Based on the sequential radiographs and three-dimensional CT images presented above, we were able to clearly monitor the degradation of the material in the bone defect area as well as new bone formation and remodeling. In Group D, because of the lack of seeded cells, the degradation of β -TCP was faster than that of the tissue-engineered bone.

Histomorphometrical Analysis of Fluorochrome Labeling

Using the technique of sequential fluorescent labeling, we clearly observed the mineralizing deposition process in the implanted grafts at each time point. As shown in Figure 5, the volume of fluorescent labeling with TE, CA, AL, and CB represented the bone mineralization and deposition at 2, 4, 7, and 11 months, respectively.

At 2 months, the volume of TE labeling (yellow) in Groups A and B was $4.72 \pm 1.29\%$ and $4.46 \pm 0.95\%$, respectively, which was less than that of Group C ($8.24 \pm 1.59\%$) but more than that of Group D ($0.82 \pm 0.24\%$) (Figure 5A–D). There were significant differences between Group C and Group A and between Group C and Group B ($p < .05$), but no difference between Group A and Group B ($p > .05$) (Figure 5E).

At 4 months, the volume of CA labeling (green) was $3.26 \pm 0.54\%$, $3.41 \pm 0.89\%$, $3.84 \pm 0.61\%$, and $1.03 \pm 0.20\%$ for Groups A, B, C, and D, respectively (Figure 5A–D). There were significant differences

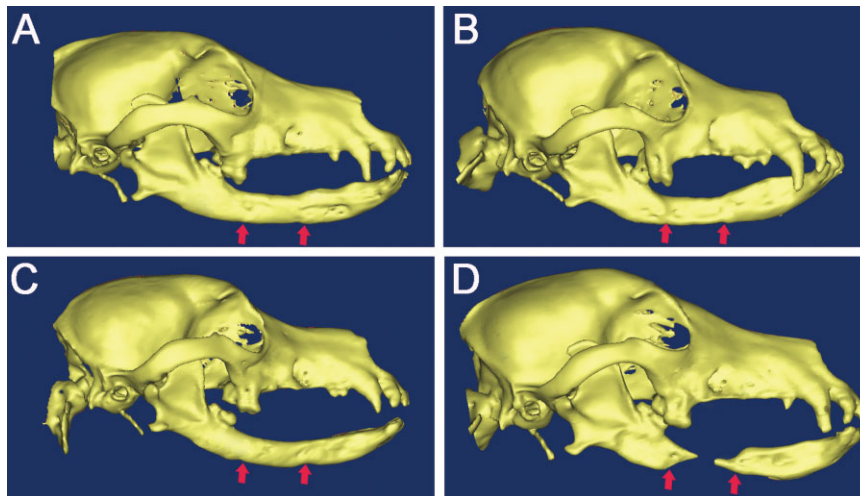


Figure 4 Three-dimensional reconstruction images of treated mandibles at 12 months post-operation. A smooth surface on the reparative tissue and continuity of the mandibles were found in Groups A, B, and C. The bone defect still existed in Group D.

between Groups A, B, and C and Group D ($p > .05$), but no significant differences among Groups A, B, and C ($p > .05$) (Figure 5E). At 7 and 11 months, the volume of AL labeling (red) and CB labeling (blue) was not significantly different among the four groups (Figure 5A–C and E).

Taken together, these data indicate that CBOs and FBOs promote bone mineralization and deposition in tissue-engineered bone and that there was no difference between the CBOs and FBOs. The two tissue-engineered constructs remained inferior to autologous bone transplantation in Group C at 2 months but caught up at 4 months.

Histological Findings

To verify the findings above, the histology of the repaired defects at 12 months post-operation was determined in non-decalcified specimens. The fraction of newly formed bone area was $62.73 \pm 12.28\%$ and $68.83 \pm 14.52\%$ in Groups A and B, respectively, which was comparable with that of Group C ($64.77 \pm 17.75\%$). No significant difference was found among these three groups ($p > .05$). However, in Group D, only a small amount of bone formation was observed (Figure 6A–D). There were significant differences between Groups A, B, and C and Group D ($p < .05$) (Figure 6E). Immunohistochemical staining also showed that the expression of OCN in Groups A, B, and C was consistent with that in Group D (Figure 7A–D).

DISCUSSION

The present study demonstrated that critically sized segmental defects of the canine mandible could be repaired by CBOs administered with biodegradable β -TCP and that the scaffold alone was not sufficient to repair such a large mandibular defect. No difference was found between CBOs and FBOs in promoting bone mineralization and deposition. These results indicate that tissue-banked CBOs may represent an accessible source of cells for large-volume bone regeneration.

Cell survival in tissue banking has been a subject of controversy in the literature, with many investigators believing that most cells in all cryopreserved grafts die.^{3,26–28} However, other studies have reported that under certain circumstances, cryopreservation techniques can maintain osteoblast viability in frozen bone.^{15,29} In this study, we isolated osteoblasts from bone that had been cryopreserved for 3 months and confirmed that the CBOs had an osteogenic phenotype according to alkaline phosphatase, alizarin red S calcium nodule staining, RT-PCR, and immunohistochemistry in vitro. In addition, we also successfully repaired a segmental mandibular defect using CBOs combined with β -TCP. In this respect, the use of CBOs in bone regeneration may broaden the application of the current cryopreserved grafts in tissue banking.

It has been reported that postoperative radiographs are able to show radiopacity changes in transplanted grafts, and thus x-ray examination may be an effective

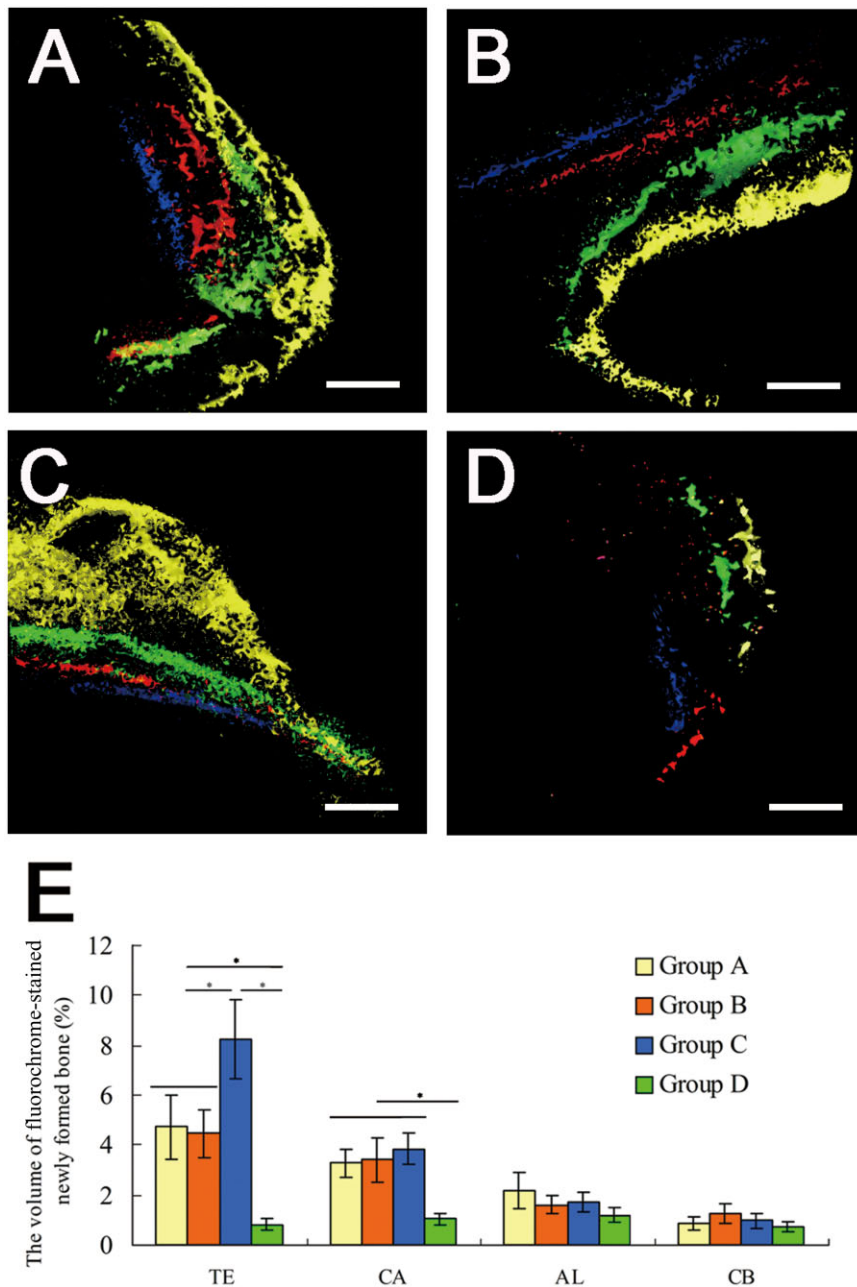


Figure 5 Three-dimensional reconstruction images of fluorescent labeling. Fluorescent labeling of tetracycline hydrochloride (TE, yellow) in Groups A, B, C, and D at 2 months is shown in A–D. There were significant differences among the groups receiving tissue-engineered bone (Groups A and B), autogenous bone (Group C), and beta-tricalcium phosphate alone (Group D) ($p < .05$), but no difference was observed between Groups A and B ($p > .05$). A significant difference was also found between the tissue-engineered bones and autogenous bone. At 4 months, the fluorescent labeling of calcein (CA, green) was not significantly different among Groups A, B, and C. There was a significant difference between Group D and Groups A, B, and C (A–D). At 7 and 11 months, the fluorescent labeling of alizarin red S (AL, red) and calcein blue (CB, blue) was not significantly different among the four groups (A–D); scale bar = 30 μ m. The graph demonstrates the volume analysis of each fluorescent label in the four groups (E). * $p < .05$.

method to evaluate new bone formation in the bone defect area.^{30,31} In the current study, we monitored new bone mineralization and deposition through periodic radiographs. At 1 month after surgery, in Groups A, B, and C, there was no obvious new bone formation in

the segmental bone defect. The interfaces between the implants and bone ends were clear. At 5 months post-operation, the radiopacity in the implants began to be obvious in Groups A, B, and C, and the granular texture of the implants in Groups A and B became blurred, with

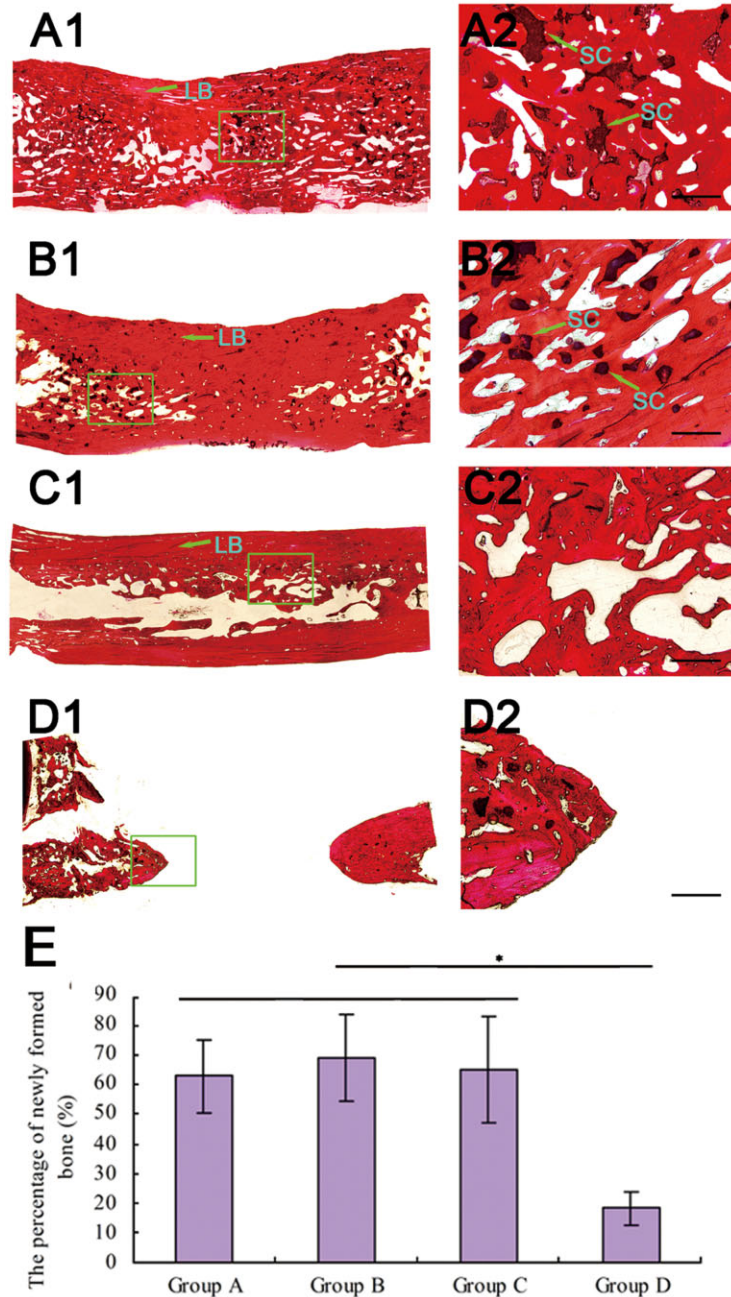


Figure 6 Non-decalcified samples of the repaired mandible at 12 months post-operation. The macroscopic view of the repaired area in each group is shown: Group A (A), Group B (B), Group C (C), and Group D (D). Detail views of the inside area (solid frame; A2, B2, C2) were obtained at high magnification (scale bar = 1,000 μ m). In Groups A and B, bone defects were repaired with a large amount of newly formed bone together with some nondegraded beta-tricalcium phosphate particles at the interfacial and inside areas (A1 and B1; arrow shows lamellar bone, LB; A2 and B2, arrow shows the scaffold, SC). In Group C, bony union also occurred at the interfacial and inside areas (C1 and C2). In Group D, minimal new bone was found at the inside area, and the bone defect was not repaired (D1 and D2). There were significant differences between Groups A, B, and C and Group D. The graph showed the analysis of newly formed bone area in the four groups (E). * $p < .05$.

the gaps between the implants and bone ends disappearing. These results indicate that bone mineralization and deposition occurred inside the implants in the three groups. In comparison, in Group D, the amount of β -TCP decreased dramatically because of degradation,

and distinct radiolucent areas were obvious around the implant. At 11 months post-operation, in Groups A, B, and C, continuity of the mandible was achieved, and the implants appeared smoother and more radiopaque. These findings are also consistent with the results

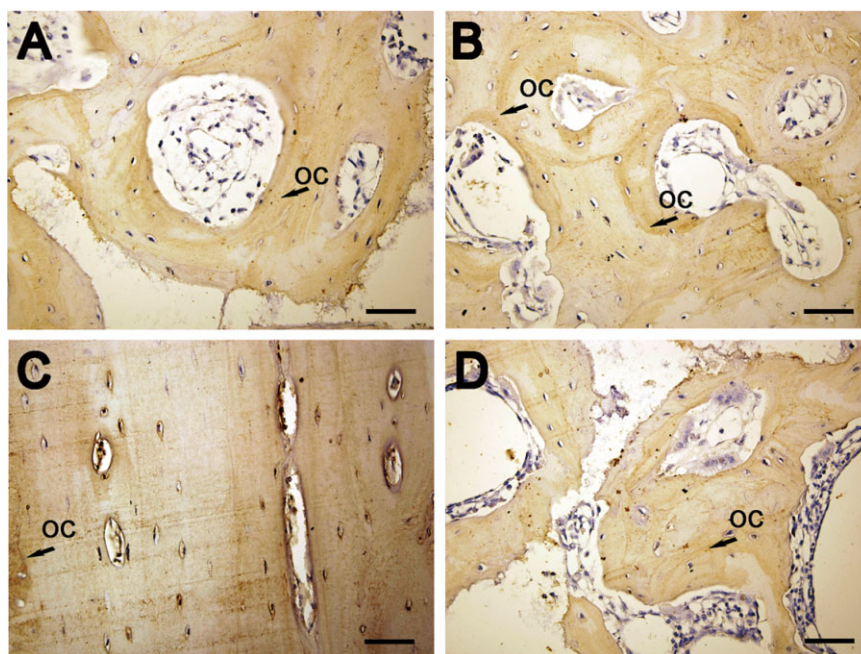


Figure 7 Osteocalcin immunohistochemistry of new bone formation in Groups A (A), B (B), C (C), and D (D) at 12 months post-operation (scale bar = 150 μ m). The expression of osteocalcin in Groups A, B and C displayed intensive osteocalcin staining in the bone matrix, which was consistent with that of Group D (arrow shows osteocalcin staining, OC).

reported in our previous studies and the studies of other groups.^{25,30}

The technique of fluorescent labeling may be useful for monitoring bone mineralization and deposition in the implant.^{32–34} According to different colors of fluorescent staining, we calculated the amount of new bone deposition at specific time points. At 2 months after surgery, in Groups A and B, which received implanted seeded cells, the volume of TE staining was higher than that of Group D but still lower than that of Group C, possibly because the autogenous bone provided a large number of osteoblasts and cytokines and a natural structure, which therefore improved the speed of bone mineralization at the early stage, whereas the migration of native osteoblasts only without any transplanted cells in the group that received β -TCP produced less bone mineralization.³⁵ We did not observe any differences between Groups A and B at this time point. In comparison, because of the lack of seeded cells, the volume of fluorescent labeling in Group D was much less than that in Groups A, B, and C at 2 months post-operation. At 4 months, though higher bone mineralization was seen in Group C at 2 months, the volume of fluorescent labeling was comparable with the patterns seen in Groups A and B. No significant differences were found in the volume of AL or CB among the four groups with long-term

observation. These results indicate that CBOs and FBOs had a similar ability to promote osteogenesis and that the use of tissue-engineered bone enhanced the speed of bone mineralization and deposition.

As shown in the non-decalcified specimens, woven bone formation was observed more frequently in the center of the tissue-engineered bone; at the edge of the implant, lamellar bone was more common, which is consistent with findings reported from other groups.³⁶ The structure of the regenerated bones may be related to mechanical forces in the oral cavity.³⁷ To further determine the characteristics of the implanted grafts in Groups A, B, and C, we evaluated the expression of OCN in the three groups. OCN has been reported to play an important role in bone formation and remodeling processes, and thus its expression could be used to assess the properties of the tissue-engineered bone.³⁸ We found that OCN expression was consistent in Groups A, B, and C, which indicates that the characteristics of these bones were similar and also suggests that the tissue-engineered bones still underwent bone remodeling.³⁰ As the regenerated bones had not been completely remodeled into a normal mandible, long-term follow-up was still needed to determine whether the engineered bones in Groups A and B could be remodeled into a normal mandibular structure.

With respect to bone regeneration, some groups have reported that the scaffold can achieve bone reconstruction without seeding of osteogenic cells.^{19,39} Based on three-dimensional CT images, we found that bony union was achieved in Group A, implanted with CBOs, and Group B, implanted with FBOs, but that nonunion and minimal callus occurred in Group D. We therefore propose that only small defects, and not large defects, could be repaired with the scaffold alone.⁴⁰ In small defects, native cells could migrate into the scaffold to generate new tissues and achieve bony union. In large defects, however, the migration rate of native cells was not high to match the degradation of the scaffold. Accordingly, osteoconductive β -TCP alone only achieved a delayed and less effective mineralization in the segmental mandibular defect region in Group D.²⁵ The data also confirm that seeded cells implanted in a scaffold could promote new bone formation.^{41,42}

In this experiment, we provide direct evidence for the application of CBOs combined with scaffolds for bone regeneration in a preclinical evaluation. Moreover, through the fabrication of tissue-engineered bone using CBOs combined with a large volume of customized scaffold, we avoided the limitations of bone tissue banking resources and the limitations of the cryopreserved bone shape for bone regeneration. Because the use of cells derived from frozen tissue may prevent age-related decreases in cell functionality,¹⁷ we may still be able to regenerate a large volume of bone when the regenerative potential of the body has decreased with aging.

In summary, this study demonstrated that CBOs combined with β -TCP could promote bone mineralization and deposition, that tissue-engineered bone could repair critically sized mandibular defects in a large animal model, and that there was no significant difference between CBOs and FBOs in promoting osteogenesis *in vivo*. Furthermore, the results above also suggest that CBOs may be a reliable cell source for bone tissue regeneration. The application of CBOs was an effective approach for the clinical reconstruction of segmental mandibular defects.

ACKNOWLEDGMENTS

This work was supported by the National Natural Science Foundation of China (81271114, 81200815, 81271182, 81070848, 81202131, 81100788); National Basic Research Program of China (973 Program, 2012CB9 33604); Science and Technology Fund, Shanghai Jiao

Tong University School of Medicine (11XJ21024); and the High-tech Research and Development Program of China (2012AA030309).

REFERENCES

1. Cancedda R, Giannoni P, Mastrogiacomo M. A tissue engineering approach to bone repair in large animal models and in clinical practice. *Biomaterials* 2007; 28:4240–4250.
2. Voss P, Sauerbier S, Wiedmann-Al-Ahmad M, et al. Bone regeneration in sinus lifts: comparing tissue-engineered bone and iliac bone. *Br J Oral Maxillofac Surg* 2010; 48:121–126.
3. Oh JH, Zoller JE, Kubler A. A new bone banking technique to maintain osteoblast viability in frozen human iliac cancellous bone. *Cryobiology* 2002; 44:279–287.
4. Reuther T, Kettmann C, Scheer M, Kochel M, Iida S, Kubler AC. Cryopreservation of osteoblast-like cells: viability and differentiation with replacement of fetal bovine serum *in vitro*. *Cells Tissues Organs* 2006; 183:32–40.
5. Mangano C, Piattelli A, Mangano A, et al. Combining scaffolds and osteogenic cells in regenerative bone surgery: a preliminary histological report in human maxillary sinus augmentation. *Clin Implant Dent Relat Res* 2009; 11(Suppl 1):e92–102.
6. Kneser U, Schaefer DJ, Polykandriotis E, Horch RE. Tissue engineering of bone: the reconstructive surgeon's point of view. *J Cell Mol Med* 2006; 10:7–19.
7. Zigdon-Giladi H, Bick T, Lewinson D, Machtei EE. Co-transplantation of endothelial progenitor cells and mesenchymal stem cells promote neovascularization and bone regeneration. *Clin Implant Dent Relat Res* 2013. DOI:10.1111/cid.12104
8. Zhao J, Zhang Z, Wang S, et al. Apatite-coated silk fibroin scaffolds to healing mandibular border defects in canines. *Bone* 2009; 45:517–527.
9. Risbud MV, Shapiro IM. Stem cells in craniofacial and dental tissue engineering. *Orthod Craniofac Res* 2005; 8:54–59.
10. Zuk PA. Tissue engineering craniofacial defects with adult stem cells? Are we ready yet? *Pediatr Res* 2008; 63:478–486.
11. Machado E, Fernandes MH, Gomes PS. Dental stem cells for craniofacial tissue engineering. *Oral Surg Oral Med Oral Pathol Oral Radiol* 2012; 113:728–733.
12. Pre D, Ceccarelli G, Gastaldi G, et al. The differentiation of human adipose-derived stem cells (hASCs) into osteoblasts is promoted by low amplitude, high frequency vibration treatment. *Bone* 2011; 49:295–303.
13. Pu LL. Cryopreservation of adipose tissue. *Organogenesis* 2009; 5:138–142.
14. Ma L, Makino Y, Yamaza H, et al. Cryopreserved dental pulp tissues of exfoliated deciduous teeth is a feasible stem cell resource for regenerative medicine. *PLOS ONE* 2012; 7:e51777.

15. Reuther T, Rohmann D, Scheer M, Kubler AC. Osteoblast viability and differentiation with Me₂SO as cryoprotectant compared to osteoblasts from fresh human iliac cancellous bone. *Cryobiology* 2005; 51:311–321.
16. Simpson D, Kakarala G, Hampson K, Steele N, Ashton B. Viable cells survive in fresh frozen human bone allografts. *Acta Orthop* 2007; 78:26–30.
17. Wang S, Zhao J, Zhang W, et al. Maintenance of phenotype and function of cryopreserved bone-derived cells. *Biomaterials* 2011; 32:3739–3749.
18. Zerbo IR, Bronckers AL, de Lange GL, van Beek GJ, Burger EH. Histology of human alveolar bone regeneration with a porous tricalcium phosphate. A report of two cases. *Clin Oral Implants Res* 2001; 12:379–384.
19. Horch HH, Sader R, Pautke C, Neff A, Deppe H, Kolk A. Synthetic, pure-phase beta-tricalcium phosphate ceramic granules (Cerasorb) for bone regeneration in the reconstructive surgery of the jaws. *Int J Oral Maxillofac Surg* 2006; 35:708–713.
20. Ogoose A, Hotta T, Kawashima H, et al. Comparison of hydroxyapatite and beta tricalcium phosphate as bone substitutes after excision of bone tumors. *J Biomed Mater Res B Appl Biomater* 2005; 72:94–101.
21. Jiang X, Zhao J, Wang S, et al. Mandibular repair in rats with premineralized silk scaffolds and BMP-2-modified bMSCs. *Biomaterials* 2009; 30:4522–4532.
22. Wang S, Zhang Z, Xia L, et al. Systematic evaluation of a tissue-engineered bone for maxillary sinus augmentation in large animal canine model. *Bone* 2010; 46:91–100.
23. Sun XJ, Zhang ZY, Wang SY, Gittens SA, Jiang XQ, Chou LL. Maxillary sinus floor elevation using a tissue-engineered bone complex with OsteoBone and bMSCs in rabbits. *Clin Oral Implants Res* 2008; 19:804–813.
24. Wang S, Zhang W, Zhao J, et al. Long-term outcome of cryopreserved bone-derived osteoblasts for bone regeneration in vivo. *Biomaterials* 2011; 32:4546–4555.
25. Wang S, Zhang Z, Zhao J, et al. Vertical alveolar ridge augmentation with beta-tricalcium phosphate and autologous osteoblasts in canine mandible. *Biomaterials* 2009; 30:2489–2498.
26. Song YC, Khirabadi BS, Lightfoot F, Brockbank KG, Taylor MJ. Vitreous cryopreservation maintains the function of vascular grafts. *Nat Biotechnol* 2000; 18:296–299.
27. Karlsson JO. Cryopreservation: freezing and vitrification. *Science* 2002; 296:655–656.
28. Nagy ZP, Chang CC, Shapiro DB, Bernal DP, Kort HI, Vajta G. The efficacy and safety of human oocyte vitrification. *Semin Reprod Med* 2009; 27:450–455.
29. Heyligers IC, Klein-Nulend J. Detection of living cells in non-processed but deep-frozen bone allografts. *Cell Tissue Bank* 2005; 6:25–31.
30. Yuan J, Zhang WJ, Liu G, et al. Repair of canine mandibular bone defects with bone marrow stromal cells and coral. *Tissue Eng Part A* 2010; 16:1385–1394.
31. Cancedda R, Cedola A, Giuliani A, et al. Bulk and interface investigations of scaffolds and tissue-engineered bones by X-ray microtomography and X-ray microdiffraction. *Biomaterials* 2007; 28:2505–2524.
32. Pautke C, Vogt S, Tischer T, et al. Polychrome labeling of bone with seven different fluorochromes: enhancing fluorochrome discrimination by spectral image analysis. *Bone* 2005; 37:441–445.
33. Fukuda S, Iida H. Effects of orchidectomy on bone metabolism in beagle dogs. *J Vet Med Sci* 2000; 62:69–73.
34. Shimomoto Y, Chung CJ, Iwasaki-Hayashi Y, Muramoto T, Soma K. Effects of occlusal stimuli on alveolar/jaw bone formation. *J Dent Res* 2007; 86:47–51.
35. Dinopoulos H, Dimitriou R, Giannoudis PV. Bone graft substitutes: what are the options. *Surgeon* 2012; 10:230–239.
36. Nair MB, Varma HK, Menon KV, Shenoy SJ, John A. Tissue regeneration and repair of goat segmental femur defect with bioactive triphasic ceramic-coated hydroxyapatite scaffold. *J Biomed Mater Res A* 2009; 91:855–865.
37. Huiskes R, Ruimerman R, van Lenthe GH, Janssen JD. Effects of mechanical forces on maintenance and adaptation of form in trabecular bone. *Nature* 2000; 405:704–706.
38. Jankovska I, Pilmane M, Urtane I. Osteopontin and osteocalcin in maxilla tissue of skeletal Class III patients. *Stomatologija* 2009; 11:125–128.
39. Browaeys H, Bouvry P, De Bruyn H. A literature review on biomaterials in sinus augmentation procedures. *Clin Implant Dent Relat Res* 2007; 9:166–177.
40. Kato E, Lemler J, Sakurai K, Yamada M. Biodegradation property of beta-tricalcium phosphate–collagen composite in accordance with bone formation: a comparative study with Bio-Oss Collagen® in a rat critical-size defect model. *Clin Implant Dent Relat Res* 2012. DOI:10.1111/j.1708-8208.2012.00467.x
41. Logeart-Avramoglou D, Anagnostou F, Bizios R, Petite H. Engineering bone: challenges and obstacles. *J Cell Mol Med* 2005; 9:72–84.
42. Chatterjea A, Meijer G, van Blitterswijk C, de Boer J. Clinical application of human mesenchymal stromal cells for bone tissue engineering. *Stem Cells Int* 2010; 2010:1–12.

Copyright of Clinical Implant Dentistry & Related Research is the property of Wiley-Blackwell and its content may not be copied or emailed to multiple sites or posted to a listserv without the copyright holder's express written permission. However, users may print, download, or email articles for individual use.